210–220 *Nucleic Acids Research, 2019, Vol. 47, No. 1* *Published online 16 November 2018*
doi: 10.1093/nar/gky1143

Single-molecule imaging of DNA gyrase activity in living *Escherichia coli*

Mathew Stracy[1,†], Adam J.M. Wollman[2,†], Elzbieta Kaja[5], Jacek Gapinski[3], Ji-Eun Lee[2], Victoria A. Leek[4], Shannon J. McKie[4], Lesley A. Mitchenall[4], Anthony Maxwell[4], David J. Sherratt[1], Mark C. Leake[2,*] and Pawel Zawadzki[1,3,*]

[1]Department of Biochemistry, University of Oxford, South Parks Road, Oxford OX1 3QU, UK, [2]Biological Physical Sciences Institute (BPSI), Departments of Physics and Biology, University of York, York YO10 5DD, UK, [3]Molecular Biophysics Division, Faculty of Physics, A. Mickiewicz University, Umultowska 85, 61-614 Poznan, Poland, [4]Department of Biological Chemistry, John Innes Centre, Norwich Research Park, Norwich NR4 7UH, UK and [5]NanoBioMedical Centre, Adam Mickiewicz University, Umultowska 85, 61-614 Poznan, Poland

Received July 12, 2018; Revised October 11, 2018; Editorial Decision October 25, 2018; Accepted November 07, 2018

ABSTRACT

Bacterial DNA gyrase introduces negative supercoils into chromosomal DNA and relaxes positive supercoils introduced by replication and transiently by transcription. Removal of these positive supercoils is essential for replication fork progression and for the overall unlinking of the two duplex DNA strands, as well as for ongoing transcription. To address how gyrase copes with these topological challenges, we used high-speed single-molecule fluorescence imaging in live *Escherichia coli* cells. We demonstrate that at least 300 gyrase molecules are stably bound to the chromosome at any time, with ∼12 enzymes enriched near each replication fork. Trapping of reaction intermediates with ciprofloxacin revealed complexes undergoing catalysis. Dwell times of ∼2 s were observed for the dispersed gyrase molecules, which we propose maintain steady-state levels of negative supercoiling of the chromosome. In contrast, the dwell time of replisome-proximal molecules was ∼8 s, consistent with these catalyzing processive positive supercoil relaxation in front of the progressing replisome.

INTRODUCTION

The double-helical structure of DNA leads to major topological problems during DNA replication and transcription. As DNA and RNA polymerases translocate along the chromosome they cause local over-winding of DNA ahead of them; if excessive positive (+) supercoiling accumulates it can inhibit the progress of the enzymes, leading to a shutdown of these essential cell processes. Furthermore, (+) supercoiling, which accumulates ahead of the replication fork, can diffuse backwards causing entanglement of daughter chromosomes, which must be unlinked before cell division can occur. In *Escherichia coli* these topological problems are resolved by two type II topoisomerases, DNA gyrase and DNA topoisomerase (topo) IV, which are essential enzymes that change topology by introducing transient double-stranded breaks into DNA and pass a second double-stranded DNA segment through the break before resealing it (1) (Figure 1A). Gyrase, the focus of this study, is formed from a dimer of GyrA, primarily responsible for DNA binding, and two GyrB subunits, which provide the ATPase activity.

In *E. coli*, the chromosome is maintained in a negatively (−) supercoiled state, and the appropriate level of supercoiling is important for regulation of almost all processes which take place on DNA, including transcription, replication, repair and recombination (2,3). For example, the expression level of many genes, including gyrase itself, is regulated by the level of supercoiling (4). Gyrase is unique in its ability to introduce (−) supercoils into DNA, and is therefore the central enzyme responsible for maintaining supercoiling homeostasis (5–8); however, local DNA supercoiling is constantly being altered by ongoing replication, transcription and repair. The activities of gyrase must therefore be responsive to these processes taking place in different regions of the chromosome (9,10).

The most acute topological problem arises during DNA replication, which is performed by two replisomes traveling in opposite directions around the circular chromosome at speeds of up to 1000 base pairs per second (bp/s) (11,12). Without the action of type II topoisomerases, replication of the 4.6 Mb *E. coli* chromosome would result in two

*To whom correspondence should be addressed. Email: zawadzki@amu.edu.pl
Correspondence may also be addressed to Mark C. Leake. Email: mark.leake@york.ac.uk
†The authors wish it to be known that, in their opinion, the first two authors should be regarded as joint First Authors.

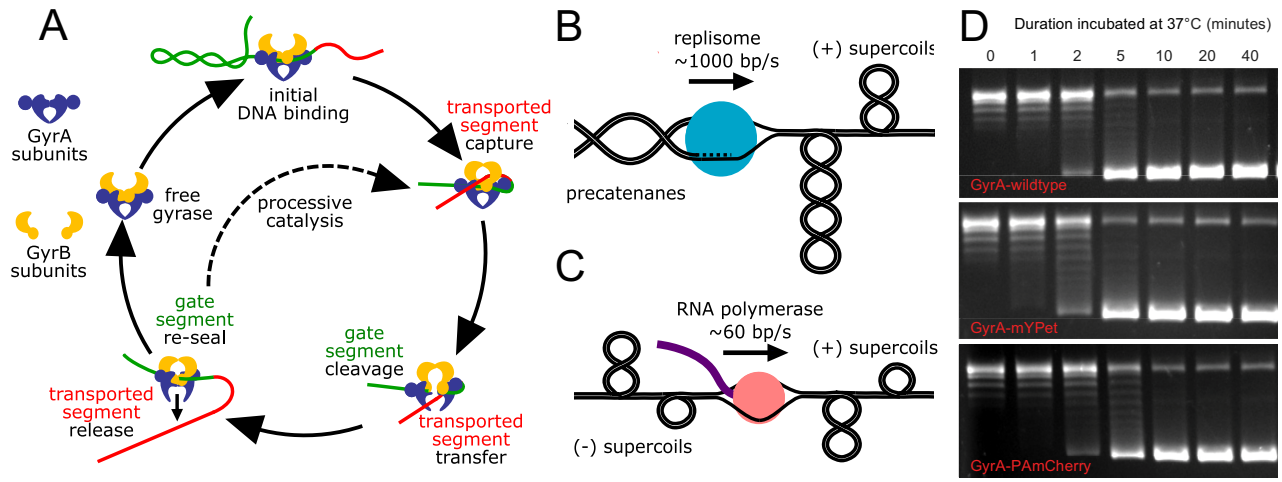

Figure 1. The activity of gyrase. (**A**) DNA gyrase catalytic cycle. (**B**) Replication introduces (+) supercoils ahead and precatenated DNA behind. Gyrase acts ahead of the fork while topo IV removes precatenanes behind. (**C**) Gyrase removes (+) supercoiling from ahead of RNAP to ensure unperturbed transcription. (**D**) Time course supercoiling assays comparing the activity of GyrA fusion proteins with wild-type GyrA after different incubation periods at 37°C. Gyrase was incubated with relaxed pBR322 DNA in standard supercoiling assays. Samples were taken at the intervals indicated and loaded onto a 1% agarose gel and analyzed by electrophoresis.

daughter chromosomes interlinked with a linking number of >440000 (given the DNA helical repeat of ∼10 bp). Type II topoisomerases change the linking number by two each catalytic cycle, and must therefore perform over 220000 catalytic events before segregation can occur. When the replisome is prevented from rotating around the DNA helix as it progresses, as originally suggested by Liu & Wang (13), (+) supercoils rapidly accumulate ahead of the replication fork. On the other hand, any rotation of the replication fork (14) allows (+) supercoils ahead of the fork to diffuse backwards forming precatenanes between the newly-replicated daughter chromosomes, which must be unlinked prior to chromosome segregation. Gyrase is inefficient in decatenation, and is believed to act ahead of the fork relaxing (+) supercoils, whereas topo IV acts preferentially behind the fork removing precatenanes (11,15,16).

To allow the replisome to maintain its incredibly high translocation rate, the two type II topoisomerases must relax up to 100 (+) supercoils per second for each fork (assuming a replisome translocation rate of 1000 bp/s, and DNA helical repeat of ∼10 bp) (Figure 1B). *In vitro,* the rate of the topoisomerase reaction for both gyrase and topo IV has been measured at ∼1 s^{-1}, with each cycle removing 2 supercoils (17–23), suggesting that ∼50 enzymes would be required per fork to keep up with the replication rate in live bacteria. Early studies of chromosome fragmentation in *E. coli* cells using the gyrase targeting drug, oxolinic acid (24), suggested that gyrase may be clustered near the replication fork. However, this raises the question of how so many gyrase enzymes can be acting ahead of the replication fork, while avoiding extremely toxic collisions with the replication machinery. In single-molecule magnetic tweezers experiments, *E. coli* gyrase was shown to act processively (18), confirming previous ensemble observations (1) and demonstrating that it is capable of performing multiple catalytic events without dissociating from DNA while relaxing (+) supercoils and introducing (−) supercoils (Figure 1A). More recent *in vitro* experiments on *Bacillus anthracis* gyrase suggests that gyrase 'bursting' activity might relax high levels of (+) supercoiling at faster rates (19). It remains to be established whether gyrase behaves processively or not *in vivo*, and whether its catalytic mode depends on the local supercoiling environment.

The action of gyrase is also essential for unperturbed transcription. Since coupling between RNA polymerase (RNAP) and (poly)ribosomes inhibits rotation of the transcription machinery, (+) supercoils accumulate ahead, and (−) supercoils behind, elongating RNAPs (Figure 1C) (7,9,25). While the rate of introduction of supercoils by a single RNAP is slow compared to replication (∼60 bp/s, or ∼6 (+) supercoils/s) (7–9), it is far more abundant. In a cell with two replisomes there are up to 2000 RNAPs (26), introducing more (+) supercoiling overall than replication, but distributed throughout the chromosome instead of accumulated in one region. The relative contribution of transcription and replication to gyrase activity is not clear.

We aimed to understand how gyrase acts in live *E. coli* cells and how topological problems arising during replication and transcription are resolved. Live cell epifluorescence showed that gyrase forms foci colocalized with active replication forks. Single-molecule Slimfield (27,28) and photoactivated-localization microscopy (PALM) (29), showed that replication-dependent gyrase clusters comprise ∼12 enzymes per replisome, while the remaining ∼300 functional immobile enzymes interacted with the chromosome elsewhere to maintain steady-state levels of (−) supercoiling. An additional ∼300 enzymes transiently interacted with dispersed regions of the chromosome. Measuring the dwell time of gyrase bound to DNA revealed that most gyrase remain immobile for ∼2 s, whereas enzymes in the vicinity of the replisome had a ∼8 s dwell time, suggesting that when an excessive (+) supercoiling is present due to the fast progression of the fork, gyrase performs multiple rounds of catalysis without dissociating from DNA.

MATERIALS AND METHODS

Bacterial strains

All strains were derivatives of *E. coli* K-12 AB1157 (30). Replacement of endogenous genes with C-terminal fluorescent fusions was performed using λ-Red recombination with an frt-flanked kanamycin resistance (kan) cassette (31) using the primers listed in Supplementary Table S1. The strains used in this study are: GyrApam (*gyrA::PAmCherry kan*); GyrBpam (*gyrB::PAmCherry kan*); PZ291 (*gyrA::mYPet kan*); PZ171 (*gyrA::PAmCherry kan, mYPet::DnaN frt*); PZ223 (*gyrA::mYPet kan, mCherry::DnaN frt*). See the Supplementary Materials and Methods for complete details of strain construction.

Sample preparation

Strains were streaked onto LB plates containing the appropriate antibiotics. Single colonies were inoculated into M9 media supplemented with 0.2% glycerol and grown overnight at 37°C to A_{600} of 0.4–0.6, diluted into fresh M9 glycerol and grown to A_{600} of 0.1. Cells were centrifuged and immobilized for imaging on 1% agarose (Bio-Rad) pads (made by mixing low-fluorescence 2% agarose in dH_2O 1:1 with 2× growth medium) between two glass coverslips (Supplementary Methods). Where indicated cells were incubated with, 10 μg/ml ciprofloxacin for 10 min prior to imaging, or 50 μg/ml rifampicin for 30 min prior to imaging.

Epifluorescence and colocalization microscopy

Wide-field epifluorescence was performed using an Eclipse TE2000-U microscope (Nikon), equipped with 100×/NA1.4 oil objective and a Cool-Snap HQ^2 CCD. For colocalization analysis, cell outlines were defined from phase contrast images using MicrobeTracker software (32). The positions of foci formed by mCherry-DnaN were established with Gaussian fitting (Supplementary Methods). Within each cell the pairwise distances between the center of the brightest GyrA-mYPet pixel and the centroid of the nearest DnaN localization were calculated in MATLAB (MathWorks) from the square root of the squares of the summed coordinates in x and y. To control for the basal level of coincidence of foci expected from a random distribution, we calculated distances between a pixel randomly positioned within the cell and the centroid of the nearest DnaN focus within the same cells. A threshold of two pixels (256 nm) was chosen to define colocalization.

Photoactivated Localization microscopy

PALM microscopy was performed using a custom-built single-molecule microscope described in the Supplementary Materials and Methods. Photoactivatable mCherry activation was controlled with a 405 nm wavelength laser, and the photoactivated fluorophores were imaged with a 561 nm laser at 15.48 ms/frame for 30000 frames. Data analysis was performed in MATLAB (MathWorks). Fluorescent signals from individual PAmCherry molecules in each frame were localized to ∼40 nm precision by elliptical Gaussian fitting. Brightfield cell images were recorded from an LED source and condenser (ASI Imaging), and cell outlines were segmented with MicrobeTracker software (32). For colocalization analysis of super-resolved gyrase localizations with the replisome, snapshots of mYPet were taken with 488 nm excitation prior to PALM imaging of PAmCherry.

Single-particle tracking and diffusion analysis

Localizations from PALM movies were linked together into trajectories using a MATLAB implementation of the algorithm described in (33). Positions were linked into a track if they appeared in consecutive frames within a window of five pixels (0.48 μm). In rare cases when multiple localizations fell within the tracking radius, tracks were linked such that the sum of step distances was minimized. We distinguished DNA-bound and diffusing proteins by calculating an apparent diffusion coefficient $D^* = \mathrm{MSD}/(4\Delta t)$ from the mean-squared displacement (MSD) for each track with at least four steps at $\Delta t = 15$ ms (34). Immobile molecules have a non-zero D^* value due to the localization uncertainty in each measurement, σ_{loc} (40 nm), which manifests as a positive offset in D^* of ∼0.1 $\mu m^2\ s^{-1}$. Errors in D^* and fractions are SEM from fitting to at least four independent experimental repeats. Significance testing was performed using two-sample t-tests of the fraction of immobile molecules extracted from these fits (Supplementary Materials and Methods).

Dwell-time distributions using long exposure times

Long duration GyrA-PAmCherry binding was recorded at low continuous 561 nm excitation intensities using 1 s exposure times. The probability of observing a particular on-time is the product of the binding time and bleaching probabilities (34). The bleaching time distributions were measured independently using a control protein, MukB-PAmCherry, whose dwell time was previously shown to be ∼1 min much greater than bleaching time (35). MukB-PAmCherry was imaged with the same imaging conditions. On-time and bleaching time distributions were fitted with single-exponential functions to extract exponential time constants t_{on} and t_{bleach}, and the binding time constant calculated as $t_{bound} = t_{on}{*}t_{bleach}/(t_{bleach} - t_{on})$. To determine binding times near the fork snapshots of mYPet-DnaN were taken prior to PALM imaging. DnaN foci were localized with Gaussian fitting and GyrA tracks within 200 nm of a focus were used for binding time analysis. The bleaching time, $t_{bleach} = 1.16 \pm 0.04$. The uncorrected t_{on} time constants from seven experimental repeats are shown in Supplementary Table S2.

Slimfield microscopy

Slimfield microscopy was performed on a dual-color custom-made laser excitation single-molecule fluorescence microscope which utilized narrow epifluorescence excitation of 10 μm full width at half maximum (FWHM) in the sample plane to generate Slimfield illumination from a 514 nm 20 mW laser passed through a ∼3× Keplerian beam de-expander. Illumination was directed onto a sample mounted on an *xyz* nanostage (Mad City Labs, the Dane

County, Wisconsin, USA). Imaging was via a custom-made color splitter utilizing a dual-pass green/red dichroic mirror centered at long-pass wavelength 560 nm and emission filters with 25 nm bandwidths centered at 542 and 594 nm (Chroma Technology Corp., Rockingham, Vermont, USA) onto an Andor iXon 128 emCCD camera, magnified to 80 nm/pixel.

For dual color imaging we acquired 10 frames of brightfield, defocused to image the cell boundary, then acquired mCherry images by exciting with 1 mW 561 nm laser until bleached after 500 frames. Then, the mYPet images were acquired, exciting with 10 mW of 514 nm laser for 500 frames. Brightfield imaging was performed with zero gain at 100 ms exposure time while single-molecule fluorescence was performed at maximum gain at 5 ms/frame, with the addition of the 561 nm laser for mCherry. Imaging of the single label mYPet-GyrA strain utilized only 514 nm laser excitation.

Stoichiometry was determined using a method which relies on step-wise photobleaching of fluorescent protein checked against surface immobilized purified mYPet using Chung–Kennedy filtration on single-molecule intensity bleach traces (28,36–42). Probability distributions for the relative displacement of GyrA-DnaN foci and for the stoichiometry of GyrA foci were rendered using kernel density estimation (KDE), a convolution of the data with a Gaussian kernel which has an advantage in objectifying the appearance of the distribution as opposed to using semi-arbitrary bin widths on a histogram plot. The kernel width was set to the appropriate experimental precision (0.7 molecules for the stoichiometry distribution and 40 nm for the distance estimates). See Supplementary Materials and Methods.

RESULTS

Gyrase foci colocalize with the replisome

To characterize gyrase activity in live cells we replaced the endogenous *gyrA* gene with a fusion to the fluorescent protein mYPet. Cells with *gyrA-mYPet* showed normal growth indicating the fusion is functional (Supplementary Figure S1A), and purified GyrA-mYPet showed normal supercoiling activity *in vitro* (Figure 1D). Using epifluorescence, gyrase formed foci in 70 ± 6% (±SD) of cells, with the remaining cells showing a diffuse fluorescent signal, consistent with gyrase localization throughout the chromosome (Figure 2).

Since gyrase is thought to remove (+) supercoils ahead of the replication fork, we constructed a strain expressing GyrA-mYPet and a replisome marker mCherry-DnaN (11). We find that the region with highest gyrase density is frequently colocalized with the replisome (Figure 2A), reflecting earlier findings from *B. subtilis* (43). To quantify colocalization we used Gaussian fitting to localize the replisome foci and examined the cumulative distributions of distances between the brightest pixel of gyrase signal and the nearest replisome focus within each cell (Figure 2B). To control for colocalization due to random coincidence we performed the same analysis with a simulated random gyrase focus position within the same cells, showing that 80 ± 4% of the brightest gyrase pixels were located within two pixels (256 nm) from the replisome, compared to 15 ± 3% from random coincidence.

In the slow growth conditions used for our experiments, a single round of replication takes only ∼2/3 of the cell doubling time, leaving a population of young cells that have not initiated replication and cells approaching division that have completed replication (Figure 2A). Since the fraction of cells lacking replication foci (∼25% identified with spotFinder (32)) was similar to the fraction of cells lacking gyrase foci (∼30%), we asked whether the presence of gyrase foci was dependent on ongoing replication; in cells without a DnaN focus only 30 ± 10% of these non-replicating cells had a distinct gyrase focus. Taken together, this analysis suggests that distinct gyrase foci are largely associated with replication forks.

Slimfield microscopy reveals gyrase clusters of ∼12 enzymes

Epifluorescence microscopy provides a description of the ensemble behavior of fluorescently-labeled proteins inside cells, however it cannot provide a quantitative assessment of protein activity at the level of individual molecules. To enable single-molecule quantification of gyrase localization we used Slimfield microscopy on GyrA-mYPet in live cell (27,44), providing a ∼40 nm spatial precision over a millisecond temporal resolution to enable blur-free analysis of individual proteins (SI Movie 1). Qualitatively, the patterns of GyrA localization with respect to DnaN (Figure 3A, Supplementary Figure S3) were similar to those observed earlier for epifluorescence (Figure 2A). Using analysis based on the integrated pixel intensity of Slimfield images (44), we quantified the GyrA copy number, giving 1300–3300 molecules per cell across all cells, which agrees broadly with earlier estimates based on immuno-gold electron microscopy of fixed *E. coli* cells (45).

To estimate the number of gyrase in localized clusters we used custom-written localization software to automatically track GyrA foci (46). We determined the stoichiometry of each as the initial focus brightness divided by the brightness of a single mYPet (36) (Materials and Methods). Given the rate of relaxation of two positive supercoils per ∼2 s previously reported for gyrase (18,21,47,48) and assuming minimal involvement of topo IV, we expected clusters to comprise of up to 50 gyrase (since 50 enzymes are required to keep up with a replication rate of 1000 bp/s). However, the intensity of these foci indicated a mean of 24 ± 2 (±SEM) GyrA molecules (i.e. just 12 ± 1 putative heterotetramer enzymes); note a key advantage of this single-molecule approach over ensemble methods is to render not just the mean value but also the full probability distribution, which we measure as having a broad range from a minimum of two molecules to over 100 per focus (Figure 3B). Using numerical integration of the overlap integral between green and red channel foci we observed that ∼85% of all foci were colocalized with DnaN, comparable to epifluorescence. The relative separation between DnaN and GyrA foci centers was not peaked at zero but instead had a mean of 135 ± 14 (±SEM) nm, exhibiting a unimodal distribution which extended up to ∼400 nm (Figure 3C), larger than the ∼50 nm replisome diameter, suggesting that gyrase does not act in tight proximity to the replisome. The hypothesis that gyrase acts at a distance from the fork might explain how collisions between the replisome and gyrase per-

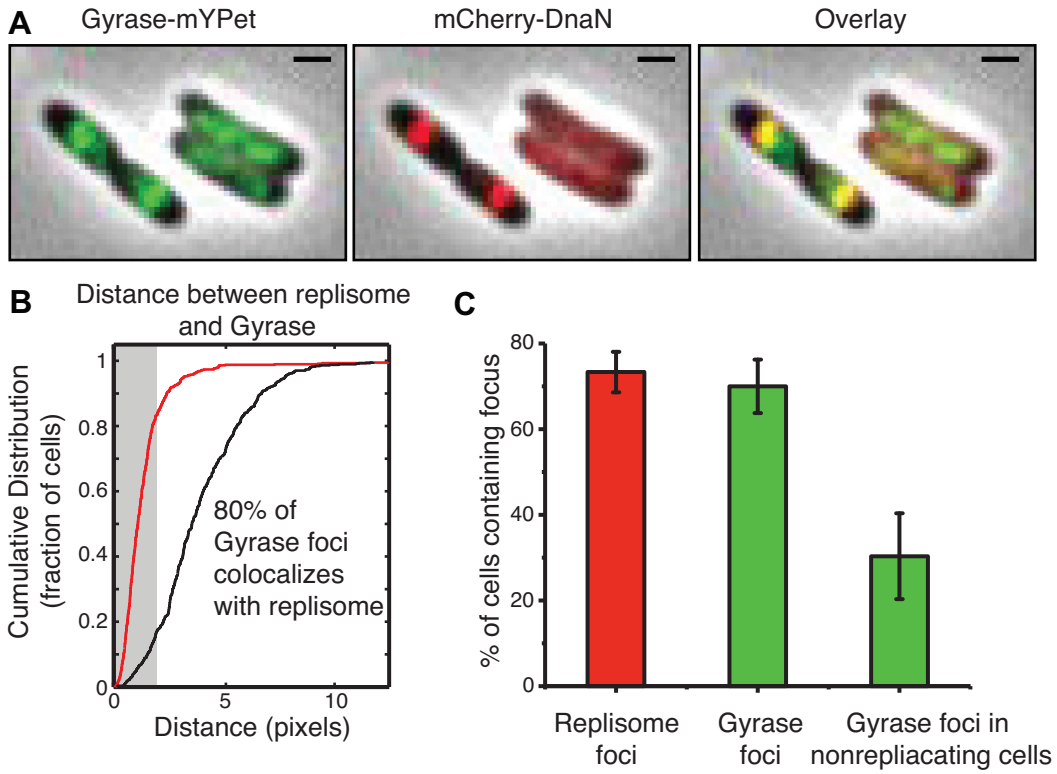

Figure 2. Epifluorescence of *E. coli* gyrase. (**A**) Example cells with gyrase, fork marked with mCherry-DnaN, and overlay of signal from both channels; scale bar 1 μm. (**B**) Cumulative distributions of distances between centroids of fork foci and brightest gyrase pixels in each cell (red), or a randomly simulated position (black). Colocalization (gray shaded rectangle) defined as when the fork centroid is ≤2 pixels (256 nm) from the brightest gyrase pixel. (**C**) % of cells from population containing fork or gyrase foci plotted as a histogram. SD error bars from $N = 3$ experiments.

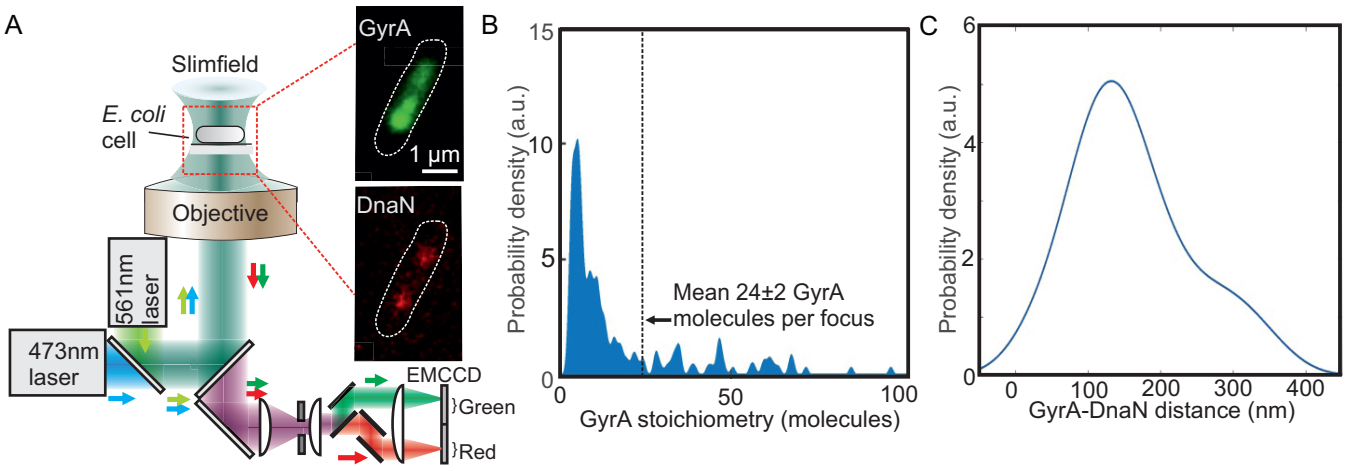

Figure 3. GyrA form foci of a few tens of molecules. (**A**) Dual-color Slimfield enables single-molecule tracking in two separate color channels with millisecond sampling, for the strain GyrA-mYPet:DnaN-mCherry, cell outline indicated (white dash). (**B**) Stoichiometry distribution rendered as a kernel density estimate (42) for all detected GyrA-mYPet foci, mean (±SEM) indicated for all GyrA, kernel width 0.7 molecules. (**C**) Distribution of displacements between foci centers for colocalized DnaN and GyrA rendered as a kernel density estimate, kernel width 40 nm. Data acquired from 72 foci using $N = 35$ cells.

forming catalysis are prevented, however we note that while DnaN forms diffraction-limited foci, it has been shown that their dissociation rate is slow and hence the focus centroid may be slightly behind the replication fork (49).

Photoactivated-localization microscopy and single-particle tracking of gyrase

To explore the mobility of single gyrase we used photoactivated-localization microscopy (PALM), combined with single-particle tracking (sptPALM) (29), enabling localization and tracking of individual GyrA by controlling the photoactivation of a photoactivable fluorescent protein such that on average one fluorophore was active per cell at any given time. We labeled GyrA genomically with photoactivable mCherry (PAmCherry) (Figure 1D, Supplementary Figure S1A) and imaged cells with a PALM microscope at 15 ms intervals for 30000 frames. Linking consecutive GyrA localizations from each frame into tracks allowed us to track gyrase movement until photobleaching (Figure 4B) (29,34).

We calculated an apparent diffusion coefficient (D^*) for each GyrA from the mean squared displacement of its track (Materials and Methods). We fitted an analytical expression (26,50) to the distribution of D^* values from all 85529 measured tracks. We found that the distribution of D^* values was best described by a three-species model, as judged using the Bayesian information criterion (BIC), giving three populations of GyrA: immobile (46 ± 5%; $D_{imm} = 0.1\ \mu m^2\ s^{-1}$ set by the localization precision), slow-diffusing (42 ± 4%; $D_{slow} = 0.25 \pm 0.01\ \mu m^2\ s^{-1}$) and fast-diffusing (12 ± 4%; $D_{fast} = 0.82 \pm 0.10\ \mu m^2\ s^{-1}$) (Figure 4C, Supplementary Figure S1B, C).

We interpret immobile tracks as DNA-bound gyrase and fast-diffusing tracks as gyrase undergoing free 3D diffusion, possibly GyrA molecules not incorporated into functional gyrase heterotetramers with GyrB. Slow-diffusing gyrases have lower mobility than expected for free 3D diffusion, consistent with transient interactions with DNA without engaging in stable binding required for catalysis.

To assess gyrase expression, we photoactivated and tracked all GyrA-PAmCherry molecules present in each cell, indicating a mean of ∼1450 ± 550 (SD) GyrA per cell (Figure 4A). We note that the copy number measured using PALM may underestimate the true copy number due to a population of PAmCherry which do not become fully photoactivatable (although this has never been characterized in bacteria) (51). Nevertheless, this estimate falls within the range estimated earlier from Slimfield microscopy, which does not use photoactivatable fluorescent proteins and hence does not suffer the same technical issue. For simplicity we have based all calculations derived from PALM experiments on the unmodified mean copy number of 1450 GyrA, but we acknowledge that the true copy number could potentially be up to 2-fold larger.

To estimate the proportion of GyrA able to form functional heterotetramers, we treated GyrA-PAmCherry cells with ciprofloxacin, which traps gyrase on DNA by stabilizing the covalently linked DNA–gyrase complex formed during catalysis (52). We find that 80 ± 3% of GyrA are immobile after drug treatment (Figure 4D), a significant increase ($p = 6 \times 10^{-5}$) from unperturbed cells and >20-fold higher than early estimates of ∼45 stabilized gyrase based on chromosome fragmentation with the much less potent quinolone, oxolinic acid (53). Since ciprofloxacin is not known to be able to capture gyrase subunits not incorporated into heterotetramers, and only stabilizes enzymes during catalysis, this demonstrates that the GyrA-PAmCherry stabilized on DNA after ciprofloxacin treatment were incorporated into functional enzymes. Assuming a copy number of 1450 GyrA subunits, of which 12% are fast-diffusing putative unincorporated subunits, our findings show that in an average cell there is enough GyrA to form ∼600 functional enzymes, of which ∼300 are DNA-bound and likely performing catalysis.

Gyrase activity in cells not undergoing replication or transcription

Epifluorescence microscopy indicates that gyrase foci are less common in cells not undergoing replication (Figure 2C). These cells show only a minimal reduction in the fraction of DNA-bound, immobile GyrA compared to replicating cells (Figures 4C and 5A) from 46 ± 5% immobile GyrA to 44 ± 5%, within statistical error, equating to a difference of just ∼15 additional gyrase enzymes per cell (with 2 replisomes), broadly consistent with Slimfield observations suggesting an average of ∼12 gyrase associated with each replisome.

We constructed a mYPet-DnaN, GyrA-PAmCherry strain to determine positions of replisomes relative to PALM-tracked gyrase (Figure 5B). The fraction of immobile gyrase 'proximal' (within 200 nm) to the replisome is 16 ± 12% which, when corrected by a fraction of simulated randomly distributed gyrase in the same region (8 ± 0.5%), equates to ∼25 more gyrase located next to both replisomes than expected from a random distribution, consistent with the small reduction of immobile gyrase observed in non-replicating cells (Figure 5A). In summary, on average only 8–12 gyrase are involved in relaxation of (+) supercoiling introduced by each replisome, and most of the remaining ∼300 DNA-bound gyrases are immobile throughout the rest of the chromosome. To test where immobile gyrase is catalytically active we treated cells with ciprofloxacin and analyzed the distribution of immobile molecules within the cells. We found immobile gyrase throughout the chromosome (Supplementary Figure S2B), suggesting that molecules close to and far from the replisome perform catalysis.

Gyrase not associated with the replisome could be relaxing (+) supercoils introduced by RNAP or be involved in maintaining steady-state levels of chromosomal (−) supercoiling. To distinguish these possibilities, we treated cells with the transcription initiation inhibitor rifampicin, resulting in a moderate reduction (by 11%) in the fraction of immobile gyrase (Figure 5C), consistent with earlier experiments which showed that rifampicin reduces plasmid supercoiling (54) Nevertheless, since 33% of gyrase remain immobile after rifampicin treatment, this suggests that gyrase performs its activity even when no (+) supercoils are being introduced due to transcription. We conclude that the role of the majority of gyrase in the cell is not directed to-

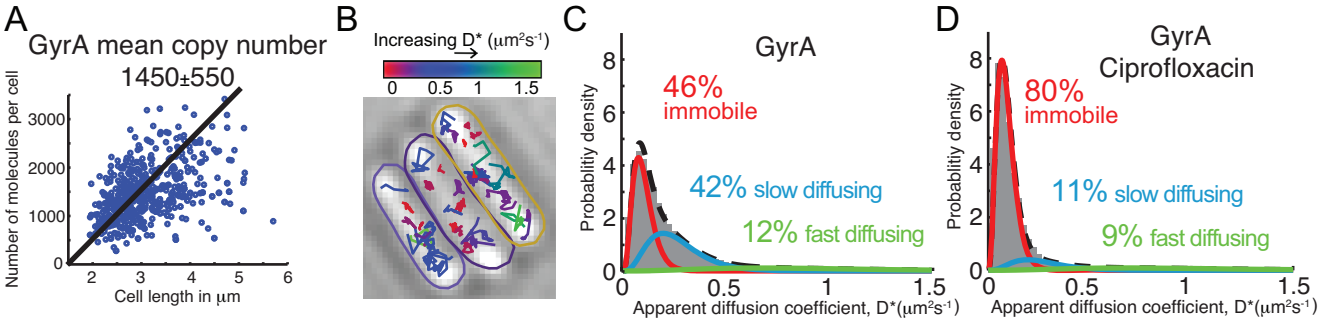

Figure 4. Intracellular characterization of *E. coli* gyrase. (**A**) Copy number of GyrA in exponentially growing culture. (**B**) Selected tracks colored according to apparent diffusion coefficient (*D**) of individual GyrA. (**C**) Distribution of *D** for 85529 tracked GyrA. (**D**) Distribution of *D** for 30813 GyrA treated for 10 min with 10 μg/ml ciprofloxacin.

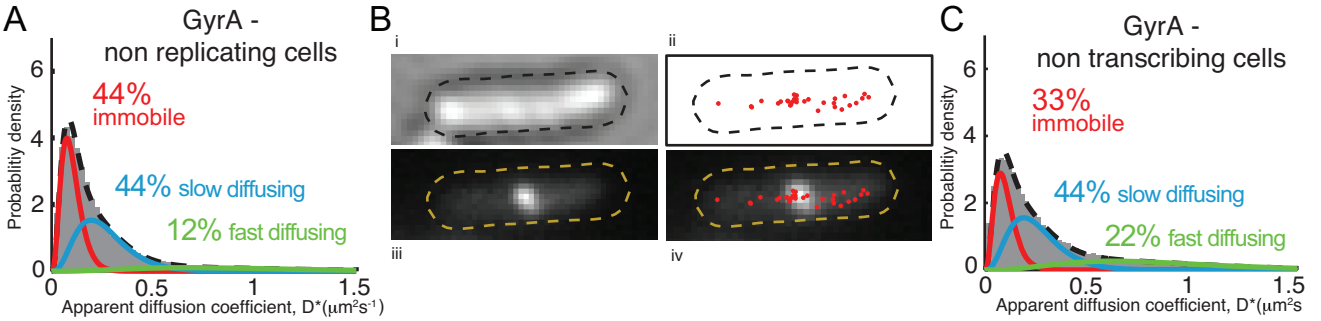

Figure 5. Effect of replication and transcription on gyrase mobility. (**A**) Distribution of *D** for 16597 tracks in cells without fork foci. (**B**) Cell (i – brightfield) with mean position of immobile molecules (ii) and position of fork marker mYPet-DnaN (iii). (iv) Superimposed images of ii and iii. (**C**) Distribution of *D** for 41 632 GyrA in cells treated for 30 min with 50 μg/ml rifampicin.

wards relaxing (+) supercoiling introduced by replication, but rather towards maintaining steady-state chromosomal supercoiling.

Different modes of gyrase

To address the conundrum of how a low number of gyrase in the vicinity of the replisome can relax up to 100 supercoils per second, we aimed to determine whether the catalytic mode depended on proximity to the replisome. To do this, we measured the binding time of gyrase inside live cells using sparse photoactivation with a low excitation intensity and long (1 s) exposure time. Under these conditions mobile gyrases are motion blurred, whereas immobile molecules appear as distinct diffraction-limited foci (34,55) (Figure 6A).

The observed dwell time for gyrase was corrected for photobleaching as described previously (34), giving a mean binding time of 2.4 ± 0.5 s (Figure 6B, Supplementary Figure S4). As a control we also measured the binding time of topo IV using a ParC-PAmCherry fusion strain from our previous study, described in reference 16. For topo IV we measured a similar binding time (1.7 ± 0.2 s), consistent with the rate of ATP hydroysis estimated in vitro for both enzymes (18,56). Ciprofloxacin resulted in a drastic increase in the fraction of immobile molecules (Figure 4D) as well as increasing the binding time, indicative of gyrase trapped during its catalytic cycle (Figure 6B). We note that the binding time estimate of ∼30 s represents the upper limit of our assay and the true binding time for gyrase after ciprofloxacin treatment may be much longer (see Supplementary Methods). We suggest that bound gyrase exhibiting binding times of ∼2.5 s are undergoing single rounds of catalytic activity, however we cannot exclude the possiblity that some gyrase bind DNA without performing catalysis.

While the observed binding time of ∼2.5 s for gyrase is not inconsistent with rates measured *in vitro* (17,18,20–23), it does not resolve the puzzle of how gyrase foci comprised of only ∼10 molecules relax (+) supercoils at a rate sufficient for replication fork progression at up to 1000 bp/s. By taking a snapshot of replication foci prior to measuring binding times, we categorized binding events taking place within ('proximal') or beyond 200 nm ('distal') from a mYPet-DnaN replisome marker. The binding time of distal gyrase (2.5 ± 0.4 s) shows no significant difference from 2.4 ± 0.5 s measured for the entire population (Figure 6C); however, proximal gyrase has a significantly longer binding time (7.7 ± 1.5 s). We propose that the longer binding time close to the replisome results from gyrase performing multiple rounds of catalytic activity without dissociating, which is facilitated by the high level of (+) supercoiling ahead of the fork.

DISCUSSION

DNA gyrase has been the subject of many biochemical and structural studies since its discovery in 1976 (1,47), however, many questions remain regarding how it acts in living cells.

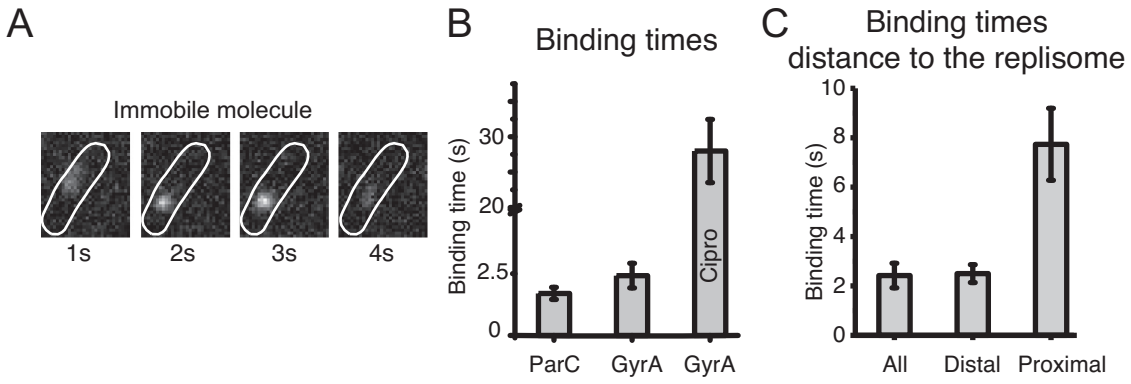

Figure 6. Binding times of gyrase inside live cells. (**A**) PALM images of an example cell imaged with 1 s exposure times; only immobile GyrA-PAmCherry produce distinct foci, while mobile GyrA are blurred and produce signal below the detection threshold. (**B**) Photobleaching-corrected binding times extracted from 1s exposures of GyrA-PAmCherry, topo IV subunit (ParC-PAmCherry) and GyrA after 10 min treatment with 10 μg/ml of ciprofloxacin. (**C**) Photobleaching-corrected binding times for GyrA, dependent on the distance from fork, categorized as proximal (<200 nm), distal (≥200 nm) or all binding events.

For example, *in vitro* gyrase can relax (+) supercoils, and also introduce (−) supercoils into relaxed DNA. Yet, little is known about what proportion of gyrase activity is directed towards different DNA substrates in the cell: removing (+) supercoiling introduced by replication, removing (+) supercoiling introduced by transcription, and maintaining steady-state (−) supercoiling of the chromosome. The relative activities of gyrase and topo IV during replication also remains a mystery. Furthermore, while *in vitro* studies have observed different modes of gyrase catalysis, it remains to be established if the catalytic mode depends on the substrate *in vivo*. In this work we have used a combination of live-cell fluorescence microscopy techniques with the aim of bridging the gap between our understanding of how gyrase acts in the test tube, to how it behaves in the native environment inside living cells. While the super-resolution techniques used in this study cannot rival the atomic-level precision of structural biology studies, placing limitations on the extent of what we can really know about the activity of any individual gyrase enzyme, they offer an order of magnitude better spatial resolution than the standard optical resolution limit, and come with the substantive advantage that it is performed in living cells and thus allows us to answer questions that are impossible to answer with structural biology or *in vitro* biochemical techniques alone, such as 'how many gyrase act in proximity to the replication fork?'

Based on PALM and Slimfield analysis we estimate that an average of ∼600 gyrase per cell are present of which ∼300 are tightly DNA-bound and presumably performing catalysis. We find that gyrase forms foci which colocalize with replisomes and comprise on average of ∼10 gyrase enzymes. In agreement with this, the fraction of DNA-bound gyrase is reduced by only a few % in cells that had either not yet initiated replication or had terminated replication but not divided. Despite the regions with the highest gyrase occupancy being close to the replisome, the vast majority of gyrase are immobile elsewhere on the chromosome. In a cell containing two replisomes there are at least ∼1000 transcribing RNAPs, introducing (+) supercoils with an overall rate up to 30-fold higher than replication (∼6000 compared to ∼200 supercoils/s) (6,26). Since we find only ∼20 out of 300 immobile gyrase are involved in relaxation of (+) supercoils introduced by replication, we expected the ∼280 remaining to participate in relaxation of (+) supercoils introduced by transcription. We find that the fraction of immobile gyrase is reduced only modestly after transcription is blocked with rifampicin, indicating that the primary activity of gyrase is instead directed towards maintaining a steady-state level of (−) supercoiling, with a caveat that rifampicin itself has a major effect on nucleoid organization through decompaction (26), which may influence gyrase activities in an unknown way. Since the time taken to transcribe an average gene is short, it is inevitable that some of the (+) and (−) supercoiling created during transcription is cancelled out after RNAP dissociation. Similarly, on highly-expressed genes (+) supercoils produced ahead of multiple RNAPs will be neutralized by (−) supercoils introduced behind. Our results show that gyrase activity should not be considered as merely removing (+) supercoils to ensure unimpeded progression of transcription and replication, but contributes to multiple interdependent processes affecting global chromosome organization and segregation.

During replication of the chromosome over 220000 catalytic events by the combined action of topo IV and gyrase must be performed, with gyrase removing (+) supercoils ahead of the replication fork and topo IV decatenating interlinked daughter chromosomes caused by diffusion of (+) supercoils behind the fork. These processes can occur simultaneously, yet the division of catalytic events between gyrase and topo IV during replication remains to be determined. Unlike gyrase, topo IV does not form foci in the proximity of the replisome (16,43,57). Nevertheless, blocking of topo IV prevents decatenation-segregation of all loci tested (11,16), demonstrating that the replisome can rotate and introduce precatenanes. Indeed, recent findings that most components of the replisome turnover every few seconds (58), suggest that the replisome is unlikely to be a barrier to replication fork rotation. The copy number of

topo IV is much lower than gyrase; our previous measurements of topo IV under the same growth conditions as this study, showed that ∼30 DNA-bound enzymes are present per cell, and the action of 1/3 of these are dependent on ongoing replication, indicating that during replication ∼10 topo IVs are performing decatenation per cell (∼5 per replication fork), most of which will be distal from the progressing forks since decatenation takes ∼12 min (16).

The combined action of ∼5 topo IV and ∼10 gyrase enzymes per replication fork is 3-fold lower that the number theoretically needed to keep up with replication rate, given the catalytic rate for both enzymes, which has been measured at ∼2 supercoil/s. Importantly, topo IV is unlikely to decatenate processively, since *in vitro* topo IV acts distributively on (−) supercoils (with the same local topology as right-handed replicative catenanes) (59,60), confirmed by our previous measurements of topo IV dwell times (16). In contrast, gyrase can remove (+) supercoils processively *in vitro* (17–19), consistent with our observations that its dwell time significantly increases close to the replisome. Previous *in vitro* measurements of the processive catalytic rate were the same as for distributive catalysis (1 supercoil/s), and thus remains insufficient to account for the rate of supercoils introduced by each replisome (up to 100 supercoil/s). Intriguingly, a recent single-molecule *in vitro* study suggests that processive relaxation of (+) supercoils by *B. anthracis* gyrase may be faster than previously measured for *E. coli* gyrase (18), with mean of ∼6 supercoils/s (19), though with individual bursts of catalysis measured as high as 107 ± 23 supercoils/s. Therefore, we suggest that the acute topological problem introduced by replication is primarily dealt with by gyrase enzymes performing processive catalysis to remove (+) supercoils ahead of replication, possibly at a higher rate than 1 supercoil/s, and we speculate that when gyrase fails to remove sufficient (+) supercoiling, replisome rotation is induced forming a substrate for topo IV behind the fork. However, it remains to be established whether *E. coli* gyrase *in vivo* can perform bursts of processive catalysis at higher rates than 1 supercoil/s.

The *E. coli* chromosome is organized into looped topological domains (8,25,61), within which supercoils can rapidly diffuse (5) and thus may delimit gyrase activity. Since the global net supercoiling of the chromosome is (−), most DNA loops will be relaxed or (−) supercoiled, and gyrase binding to these regions will perform a single round of catalysis. Our data suggest that local supercoiling may strongly influence gyrase off-rate, as we find with replication proximal gyrase remaining immobile for >8 s. Since the fork progresses at a rate of up to 1000 bp/s this would require initially binding ∼10 kb ahead of the fork to avoid collisions rather than directly ahead of it. This predicts a displacement of gyrase foci in relation to replisome position. Indeed, Slimfield analysis (Figure 3C) showed that gyrase and replisome foci are displaced by ∼100 nm. Therefore, diffusing (+) supercoils may promote processive catalysis of gyrase bound many kb away from replication, which could help to protect against detrimental gyrase-fork collisions.

Together, our results show that *in vivo* a small number of gyrase acting processively ensures unimpeded progression of the replisome, while a majority of gyrase is involved in maintaining steady-state levels of chromosome supercoiling.

DATA AVAILABILITY

Data included in full in the main text and supplementary files. Raw data available from the authors.

SUPPLEMENTARY DATA

Supplementary Data are available at NAR Online.

ACKNOWLEDGEMENTS

Author contributions: M.S., D.J.S., M.C.L. and P.Z., designed research. M.S., A.J.M.W., E.K., J.G., J.-E.L., V.A.L., S.J.M., L.A.M. and P.Z. performed experiments and analyzed data. M.S., D.J.S., M.C.L., A.M. and P.Z., wrote the paper.

FUNDING

National Science Centre Poland [2015/19/P/NZ1/03859 to P.Z.]; FNP [First TEAM/2016-1/9 to P.Z.]; Medical Research Council [MwR/K01580X/1 to M.L.]; Biotechnology and Biological Sciences Research Council [BB/N006453/1 to M.L., BB/R001235/1 to M.L. A.M., J.-E.L., BB/J004561/1, BB/P012523/1 to A.M.]; The Wellcome Trust through the Centre for Future Health at University of York [204829 to A.J.M.W.]; The Wellcome Trust [099204/Z/12Z to D.J.S.]; Sir Henry Wellcome Fellowship [204684/Z/16/Z to M.S.]; Leverhulme Trust [RP2013-K-017 to D.J.S.]; Junior Research Fellowship at Trinity College Oxford [to M.S]. Funding for open access charge: National Science Centre Poland [2015/19/P/NZ1/03859].
Conflict of interest statement. None declared.

REFERENCES

1. Bush,N.G., Evans-Roberts,K. and Maxwell,A. (2015) DNA topoisomerases. *EcoSal Plus*, **6**, doi:10.1128/ecosalplus.ESP-0010-2014.
2. Lal,A., Dhar,A., Trostel,A., Kouzine,F., Seshasayee,A.S. and Adhya,S. (2016) Genome scale patterns of supercoiling in a bacterial chromosome. *Nat. Commun.*, **7**, 11055.
3. Dorman,C.J. and Dorman,M.J. (2016) DNA supercoiling is a fundamental regulatory principle in the control of bacterial gene expression. *Biophys. Rev.*, **8**, 89–100.
4. Peter,B.J., Arsuaga,J., Breier,A.M., Khodursky,A.B., Brown,P.O. and Cozzarelli,N.R. (2004) Genomic transcriptional response to loss of chromosomal supercoiling in Escherichia coli. *Genome Biol.*, **5**, R87.
5. Koster,D.A., Crut,A., Shuman,S., Bjornsti,M.A. and Dekker,N.H. (2010) Cellular strategies for regulating DNA supercoiling: a single-molecule perspective. *Cell*, **142**, 519–530.
6. Vos,S.M., Tretter,E.M., Schmidt,B.H. and Berger,J.M. (2011) All tangled up: how cells direct, manage and exploit topoisomerase function. *Nat. Rev. Mol. Cell Biol.*, **12**, 827–841.
7. Rovinskiy,N., Agbleke,A.A., Chesnokova,O., Pang,Z. and Higgins,N.P. (2012) Rates of gyrase supercoiling and transcription elongation control supercoil density in a bacterial chromosome. *PLos Genet.*, **8**, e1002845.
8. Postow,L., Hardy,C.D., Arsuaga,J. and Cozzarelli,N.R. (2004) Topological domain structure of the Escherichia coli chromosome. *Genes Dev.*, **18**, 1766–1779.

9. Menzel,R. and Gellert,M. (1983) Regulation of the genes for E. coli DNA gyrase: homeostatic control of DNA supercoiling. *Cell*, **34**, 105–113.
10. Zechiedrich,E.L., Khodursky,A.B., Bachellier,S., Schneider,R., Chen,D., Lilley,D.M. and Cozzarelli,N.R. (2000) Roles of topoisomerases in maintaining steady-state DNA supercoiling in Escherichia coli. *J. Biol. Chem.*, **275**, 8103–8113.
11. Wang,X., Reyes-Lamothe,R. and Sherratt,D.J. (2008) Modulation of Escherichia coli sister chromosome cohesion by topoisomerase IV. *Genes Dev.*, **22**, 2426–2433.
12. Reyes-Lamothe,R., Possoz,C., Danilova,O. and Sherratt,D.J. (2008) Independent positioning and action of Escherichia coli replisomes in live cells. *Cell*, **133**, 90–102.
13. Liu,L.F. and Wang,J.C. (1987) Supercoiling of the DNA template during transcription. *PNAS*, **84**, 7024–7027.
14. Schalbetter,S.A., Mansoubi,S., Chambers,A.L., Downs,J.A. and Baxter,J. (2015) Fork rotation and DNA precatenation are restricted during DNA replication to prevent chromosomal instability. *PNAS*, **112**, E4565–E4570.
15. Joshi,M.C., Magnan,D., Montminy,T.P., Lies,M., Stepankiw,N. and Bates,D. (2013) Regulation of sister chromosome cohesion by the replication fork tracking protein SeqA. *PLos Genet.*, **9**, e1003673.
16. Zawadzki,P., Stracy,M., Ginda,K., Zawadzka,K., Lesterlin,C., Kapanidis,A.N. and Sherratt,D.J. (2015) The localization and action of topoisomerase IV in escherichia coli chromosome segregation is coordinated by the SMC complex, MukBEF. *Cell Rep.*, **13**, 2587–2596.
17. Nollmann,M., Crisona,N.J. and Arimondo,P.B. (2007) Thirty years of Escherichia coli DNA gyrase: from in vivo function to single-molecule mechanism. *Biochimie*, **89**, 490–499.
18. Nollmann,M., Stone,M.D., Bryant,Z., Gore,J., Crisona,N.J., Hong,S.C., Mitelheiser,S., Maxwell,A., Bustamante,C. and Cozzarelli,N.R. (2007) Multiple modes of Escherichia coli DNA gyrase activity revealed by force and torque. *Nat. Struct. Mol. Biol.*, **14**, 264–271.
19. Ashley,R.E., Dittmore,A., McPherson,S.A., Turnbough,C.L. Jr, Neuman,K.C. and Osheroff,N. (2017) Activities of gyrase and topoisomerase IV on positively supercoiled DNA. *Nucleic Acids Res.*, **45**, 9611–9624.
20. Ali,J.A., Jackson,A.P., Howells,A.J. and Maxwell,A. (1993) The 43-kilodalton N-terminal fragment of the DNA gyrase B protein hydrolyzes ATP and binds coumarin drugs. *Biochemistry*, **32**, 2717–2724.
21. Higgins,N.P., Peebles,C.L., Sugino,A. and Cozzarelli,N.R. (1978) Purification of subunits of Escherichia coli DNA gyrase and reconstitution of enzymatic activity. *PNAS*, **75**, 1773–1777.
22. Maxwell,A. and Gellert,M. (1984) The DNA dependence of the ATPase activity of DNA gyrase. *J. Biol. Chem.*, **259**, 14472–14480.
23. Staudenbauer,W.L. and Orr,E. (1981) DNA gyrase: affinity chromatography on novobiocin-Sepharose and catalytic properties. *Nucleic Acids Res.*, **9**, 3589–3603.
24. Drlica,K., Engle,E.C. and Manes,S.H. (1980) DNA gyrase on the bacterial chromosome: possibility of two levels of action. *PNAS*, **77**, 6879–6883.
25. Chong,S., Chen,C., Ge,H. and Xie,X.S. (2014) Mechanism of transcriptional bursting in bacteria. *Cell*, **158**, 314–326.
26. Stracy,M., Lesterlin,C., Garza de Leon,F., Uphoff,S., Zawadzki,P. and Kapanidis,A.N. (2015) Live-cell superresolution microscopy reveals the organization of RNA polymerase in the bacterial nucleoid. *Proc. Natl. Acad. Sci. U.S.A.*, **112**, E4390–E4399.
27. Plank,M., Wadhams,G.H. and Leake,M.C. (2009) Millisecond timescale slimfield imaging and automated quantification of single fluorescent protein molecules for use in probing complex biological processes. *Integr. Biol. (Camb.)*, **1**, 602–612.
28. Reyes-Lamothe,R., Sherratt,D.J. and Leake,M.C. (2010) Stoichiometry and architecture of active DNA replication machinery in Escherichia coli. *Science*, **328**, 498–501.
29. Manley,S., Gillette,J.M., Patterson,G.H., Shroff,H., Hess,H.F., Betzig,E. and Lippincott-Schwartz,J. (2008) High-density mapping of single-molecule trajectories with photoactivated localization microscopy. *Nat. Methods*, **5**, 155–157.
30. Bachmann,B.J. (1972) Pedigrees of some mutant strains of Escherichia coli K-12. *Bacteriol. Rev.*, **36**, 525–557.
31. Datsenko,K.A. and Wanner,B.L. (2000) One-step inactivation of chromosomal genes in Escherichia coli K-12 using PCR products. *Proc. Natl. Acad. Sci. U.S.A.*, **97**, 6640–6645.
32. Sliusarenko,O., Heinritz,J., Emonet,T. and Jacobs-Wagner,C. (2011) High-throughput, subpixel precision analysis of bacterial morphogenesis and intracellular spatio-temporal dynamics. *Mol. Microbiol.*, **80**, 612–627.
33. Crocker,J.C. and Grier,D.G. (1996) When like charges Attract: The effects of geometrical confinement on Long-Range colloidal interactions. *Phys. Rev. Lett.*, **77**, 1897–1900.
34. Uphoff,S., Reyes-Lamothe,R., Garza de Leon,F., Sherratt,D.J. and Kapanidis,A.N. (2013) Single-molecule DNA repair in live bacteria. *Proc. Natl. Acad. Sci. U.S.A.*, **110**, 8063–8068.
35. Badrinarayanan,A., Reyes-Lamothe,R., Uphoff,S., Leake,M.C. and Sherratt,D.J. (2012) In vivo architecture and action of bacterial structural maintenance of chromosome proteins. *Science*, **338**, 528–531.
36. Leake,M.C., Chandler,J.H., Wadhams,G.H., Bai,F., Berry,R.M. and Armitage,J.P. (2006) Stoichiometry and turnover in single, functioning membrane protein complexes. *Nature*, **443**, 355–358.
37. Leake,M.C., Greene,N.P., Godun,R.M., Granjon,T., Buchanan,G., Chen,S., Berry,R.M., Palmer,T. and Berks,B.C. (2008) Variable stoichiometry of the TatA component of the twin-arginine protein transport system observed by in vivo single-molecule imaging. *Proc. Natl. Acad. Sci. U.S.A.*, **105**, 15376–15381.
38. Delalez,N.J., Wadhams,G.H., Rosser,G., Xue,Q., Brown,M.T., Dobbie,I.M., Berry,R.M., Leake,M.C. and Armitage,J.P. (2010) Signal-dependent turnover of the bacterial flagellar switch protein FliM. *Proc. Natl. Acad. Sci. U.S.A.*, **107**, 11347–11351.
39. Wollman,A.J., Shashkova,S., Hedlund,E.G., Friemann,R., Hohmann,S. and Leake,M.C. (2017) Transcription factor clusters regulate genes in eukaryotic cells. *eLife*, **6**, e27451.
40. Miller,H., Cosgrove,J., Wollman,A.J.M., Taylor,E., Zhou,Z., O'Toole,P.J., Coles,M.C. and Leake,M.C. (2018) High-Speed Single-Molecule tracking of CXCL13 in the B-Follicle. *Front. Immunol.*, **9**, 1073.
41. Leake,M.C., Wilson,D., Bullard,B. and Simmons,R.M. (2003) The elasticity of single kettin molecules using a two-bead laser-tweezers assay. *FEBS Lett.*, **535**, 55–60.
42. Lenn,T. and Leake,M.C. (2012) Experimental approaches for addressing fundamental biological questions in living, functioning cells with single molecule precision. *Open Biol.*, **2**, 120090.
43. Tadesse,S. and Graumann,P.L. (2006) Differential and dynamic localization of topoisomerases in Bacillus subtilis. *J. Bacteriol.*, **188**, 3002–3011.
44. Wollman,A.J. and Leake,M.C. (2015) Millisecond single-molecule localization microscopy combined with convolution analysis and automated image segmentation to determine protein concentrations in complexly structured, functional cells, one cell at a time. *Faraday Discuss.*, **184**, 401–424.
45. Thornton,M., Armitage,M., Maxwell,A., Dosanjh,B., Howells,A.J., Norris,V. and Sigee,D.C. (1994) Immunogold localization of GyrA and GyrB proteins in Escherichia coli. *Microbiology*, **140**(Pt 9), 2371–2382.
46. Miller,H., Zhou,Z., Wollman,A.J. and Leake,M.C. (2015) Superresolution imaging of single DNA molecules using stochastic photoblinking of minor groove and intercalating dyes. *Methods*, **88**, 81–88.
47. Gellert,M., Mizuuchi,K., O'Dea,M.H. and Nash,H.A. (1976) DNA gyrase: an enzyme that introduces superhelical turns into DNA. *Proc. Natl. Acad. Sci. U.S.A.*, **73**, 3872–3876.
48. Reece,R.J. and Maxwell,A. (1991) DNA gyrase: structure and function. *Crit. Rev. Biochem. Mol. Biol.*, **26**, 335–375.
49. Moolman,M.C., Krishnan,S.T., Kerssemakers,J.W., van den Berg,A., Tulinski,P., Depken,M., Reyes-Lamothe,R., Sherratt,D.J. and Dekker,N.H. (2014) Slow unloading leads to DNA-bound beta2-sliding clamp accumulation in live Escherichia coli cells. *Nat. Commun.*, **5**, 5820.
50. Vrljic,M., Nishimura,S.Y., Brasselet,S., Moerner,W.E. and McConnell,H.M. (2002) Translational diffusion of individual class II MHC membrane proteins in cells. *Biophys. J.*, **83**, 2681–2692.
51. Durisic,N., Laparra-Cuervo,L., Sandoval-Alvarez,A., Borbely,J.S. and Lakadamyali,M. (2014) Single-molecule evaluation of

fluorescent protein photoactivation efficiency using an in vivo nanotemplate. *Nat. Methods*, **11**, 156–162.
52. Collin,F., Karkare,S. and Maxwell,A. (2011) Exploiting bacterial DNA gyrase as a drug target: current state and perspectives. *Appl. Microbiol. Biotechnol.*, **92**, 479–497.
53. Snyder,M. and Drlica,K. (1979) DNA gyrase on the bacterial chromosome: DNA cleavage induced by oxolinic acid. *J. Mol. Biol.*, **131**, 287–302.
54. Drlica,K., Franco,R.J. and Steck,T.R. (1988) Rifampin and rpoB mutations can alter DNA supercoiling in Escherichia coli. *J. Bacteriol.*, **170**, 4983–4985.
55. Stracy,M., Uphoff,S., Garza de Leon,F. and Kapanidis,A.N. (2014) In vivo single-molecule imaging of bacterial DNA replication, transcription, and repair. *FEBS Lett.*, **588**, 3585–3594.
56. Charvin,G., Bensimon,D. and Croquette,V. (2003) Single-molecule study of DNA unlinking by eukaryotic and prokaryotic type-II topoisomerases. *Proc. Natl. Acad. Sci. U.S.A.*, **100**, 9820–9825.
57. Nicolas,E., Upton,A.L., Uphoff,S., Henry,O., Badrinarayanan,A. and Sherratt,D. (2014) The SMC complex MukBEF recruits topoisomerase IV to the origin of replication region in live Escherichia coli. *mBio*, **5**, e01001–e01013.
58. Beattie,T.R., Kapadia,N., Nicolas,E., Uphoff,S., Wollman,A.J., Leake,M.C. and Reyes-Lamothe,R. (2017) Frequent exchange of the DNA polymerase during bacterial chromosome replication. *eLife*, **6**, e21763.
59. Crisona,N.J., Strick,T.R., Bensimon,D., Croquette,V. and Cozzarelli,N.R. (2000) Preferential relaxation of positively supercoiled DNA by E. coli topoisomerase IV in single-molecule and ensemble measurements. *Genes Dev.*, **14**, 2881–2892.
60. Stone,M.D., Bryant,Z., Crisona,N.J., Smith,S.B., Vologodskii,A., Bustamante,C. and Cozzarelli,N.R. (2003) Chirality sensing by Escherichia coli topoisomerase IV and the mechanism of type II topoisomerases. *Proc. Natl. Acad. Sci. U.S.A.*, **100**, 8654–8659.
61. Lioy,V.S., Cournac,A., Marbouty,M., Duigou,S., Mozziconacci,J., Espeli,O., Boccard,F. and Koszul,R. (2018) Multiscale structuring of the E. coli chromosome by nucleoid-associated and condensin proteins. *Cell*, **172**, 771–783.e718.